Integrated Microwave Antenna/Sensor for Sensing and Communication Applications

Tanjir Alam, *Graduate Student Member, IEEE*, and Michael Cheffena

***Abstract*— In this article, a dual-functional microwave system with a single input port that can simultaneously be used for antenna and sensor applications is presented. The dual-functional ability of the proposed system is achieved by integrating a two-port microwave sensor and a Wi-Fi antenna with a novel frequency-selective multipath filter (FSMF). The FSMF ensures efficient system operation by not affecting the operational bandwidth of the communicating antenna in the presence of different sensed materials under test (MUTs) on top of the sensor. The proposed microwave sensor also has a unique capability of measuring one more sensing parameter in addition to the often used reflection and transmission coefficients. The additional parameter is the frequency distance of two closely spaced resonance frequencies of the microwave sensor in the presence of an MUT. Compared to existing state-of-the-art techniques, the additional sensing parameter (as done in this work) can be used as an alternative to transmission coefficient for characterization of different MUTs or as an additional parameter giving more degree of freedom. The entire system is designed in a single substrate with a common input source. The performance of the dual-functional system was tested using different MUTs and showed a good agreement with the measurement results.**

***Index Terms*— Antenna sensor, filtenna, filter, microstrip antenna, microwave sensor, Wi-Fi.**

I. Introduction

MICROWAVE sensors have become popular over the last few years. Their contactless sensing capability, real-time detection ability, accuracy in measurement, ease of fabrication, and robustness have made them one of the fundamental choices in smart sensing applications. In addition, having a higher operational frequency reduces their footprint, and their planar structure allows them to integrate easily with wireless communication systems. Furthermore, compared to other types of sensors such as electrochemical [1], electroconductive [2], and chemoresistive [3], microwave sensors do not need additional energy sources for absorption and desorption of a target analyte as the microwave frequency itself can be used as a heating source [4], [5], [6]. These advantages make them amenable for various sensing applications at room temperature.

Manuscript received 11 May 2022; revised 20 June 2022 and 18 July 2022; accepted 1 August 2022. Date of publication 24 August 2022; date of current version 4 November 2022. This work was supported by the Research Council of Norway under Project 300989. *(Corresponding author: Michael Cheffena.)*

The authors are with the, Faculty of Engineering, Norwegian University of Science and Technology (NTNU), N-2815 Gjøvik, Norway (e-mail: tanjir.alam@ntnu.no; michael.cheffena@ntnu.no).

Color versions of one or more figures in this article are available at https://doi.org/10.1109/TMTT.2022.3199242.

Digital Object Identifier 10.1109/TMTT.2022.3199242

Extensive use of nonrenewable fossil fuels (such as coal and oil) in energy sectors, manufacturing industries, and day-to-day life applications raises significant concerns about the earth's atmosphere and people's health by emitting greenhouse gases and harmful particulate matter into the environment. Therefore, more and more, the use of cleaner renewable energy sources has become very essential. In this regard, biomass-made ethanol can be a great alternative choice [7]. Ethanol has a good potential to be used alone or with some other combustible fuels [8]. Hence, oil quality monitoring for using ethanol-aided gasoline becomes important as different ethanol concentrations in the ethanol–gasoline blend can cause different amounts of evaporative emissions from a vehicle exhaust system [9], [10]. Another vital role of oil quality monitoring can be measuring the moisture content of oil [11], as the higher moisture content in gasoline can severely impact the performance of the industrial machinery and its engines [12] (it can even cause permanent damage). Thus, monitoring the quality of the oil also becomes very important to ensure the safer operation of the equipment. In the following, the state of the art in microwave sensors along with our contribution beyond the state of the art is discussed.

A. State of the Art

A two-port microwave sensor can efficiently improve the sensing performance by measuring two different parameters simultaneously, i.e., the resonance frequency and the transmission coefficient. Hence, it can be a potential choice for material characterization [13], [14]. It is shown that the overall sensitivity of a microwave sensor for material characterization can be enhanced by loading complementary split-ring resonators (CSRRs) in a microstrip line. It is also possible to tune these two-port sensors utilizing a 3-D printed channel on microwave split-ring resonators (SRRs) [15]. This tuning property of a two-port microwave device can be used for sensing different dielectric materials using multiple resonators [16]. For example, in space vehicles, it is crucial to control the attitude of several machines (including the reaction wheels) and measure the torque using an angular displacement sensor. Microwave sensors can be efficient for precisely measuring the angular rotation utilizing the polarization of the electromagnetic wave [17], [18], [19]. The selectivity of microwave sensors for a particular analyte can be enhanced by incorporating a sensitive material on the microwave resonator [20], [21], [22]. The position of the deposited sensitive material

TABLE I
COMPARISON WITH EXISTING MICROWAVE SENSORS

Ref.	Ports/ Type of sensor	Measuring parameters	Operation	Shown frequency of operation [GHz]	Range of RSF shift [GHz]	Dielectric characterization	Permittivity range
[16]	2-port/ MS	Two: TC and RSF	Sensor	1-5	3.3-3.9	Yes	ϵ'=2.2-10.2
[20]	2-port/ MS	Two: TC and RSF	Sensor	1.95-2.95	2.4-2.45	No	N/A
[22]	2-port/ MS	Two: TC and RSF	Sensor	8.5-10	9.26-9.57	No	N/A
[23]	2-port/ MS	Two: TC and RC	Sensor	2-8	N/A	No	N/A
[24]	2-port/ MS	Two: TC and RC	Sensor	2-8	N/A	No	N/A
[30]	2-port/ MS	Two: TC and RSF	Sensor	1-3	1.18-1.79	Yes	ϵ'=10-80
[26]	2-port/ MS	Two: TC and RSF	Sensor	0.8-2.2	1.26-1.8	Yes	ϵ'=10-80
[27]	2-port/ MS	Two: TC and RC	Sensor	1-18	N/A	Yes	ϵ'=3-36
[28]	2-port/ MS	Two: TC and RSF	Sensor	2-6	N/A	No	N/A
[29]	2-port/ MS	One: TC	Sensor	2-2.8	2.264-2.639	No	N/A
[31]	1-port/ AS	One: RSF	Sensor	4.5-6.3	5.86-5.88	No	N/A
[32]	1-port/ AS	One: RC	Sensor	6.75-6.84	6.808-6.810	No	N/A
[33]	1-port/ AS	One: RC	Sensor	2.1-2.9	2.35-2.68	No	N/A
*TW	2-port/ multi	[a]Three	Dual-function	2-6	[b]4.02-5.03, [c]4.17-5.11	Yes	ϵ'=2.3-26

[a]RC, TC, and the frequency distance of two closely spaced resonance frequencies; [b]first RSF; [c]second RSF. N/A: Not Applicable/Available, MS: Microwave Sensor, AS: Antenna Sensor, TC: Transmission Coefficient, RC: Reflection Coefficient, RSF: Resonance Frequency.

film on the microwave resonator is essential for sensing performance. In [20], a microwave resonator-based humidity sensor has been coupled with a conducting polymer PEDOT: PSS near the high electric field region. At different humidity conditions, the amount of water absorbed by the sensitive material changes the dielectric property of the material accordingly. This change in the dielectric property of the sensing material alters the response of the microwave sensor. Similarly, these types of sensors are also very convenient for gas sensing applications [22], [23], [24] as gas sensors based on other technologies often need external energy sources [1], [2], such as a high-temperature system for absorption and desorption of the target analyte. The inclusion of such a system increases the overall cost [22]. The most important advantage of microwave sensors is that they do not need external energy sources as the microwave frequency itself can be used as a heating source [4], [5], [6] for faster absorption and desorption of the gas analyte. In [22], a microwave SRR sensor was reported for methanol gas detection by coating the inner ring of the SRR with carbon nanotube-coated fiber. Microwave sensors utilizing the interdigital capacitor (IDC) can also become a potential choice for the detection of ammonia (NH_3) by properly depositing the sensitive materials on top of the IDC [23], [24]. Besides these, there are several other microwave sensors for liquid detection [25], [26], [27], gas sensing [28], or coating defect detection [29] reported in the literature. A comparison with existing microwave sensors is summarized in Table I.

B. Contribution Beyond the State of the Art

The state-of-the-art works mentioned above have mainly two sensing parameters, i.e., the reflection and transmission coefficients. However, adding one more sensing parameter can enhance the sensor's performance, giving it a higher degree of freedom. On the other side, despite several other advantages, microwave sensors are usually designed as a single stand-alone system. Therefore, integrating a microwave sensor with other microwave components in the same substrate can provide a multifunctional microwave system. However, the perturbation of the electric field of a microwave sensor in the presence of different materials under test (MUTs) shifts its resonance frequency. This resonance frequency shift can also affect (alter) the operational bandwidth of other microwave devices connected to it. Due to this, integrating a microwave sensor with, e.g., a fixed band antenna, can change the antenna's operational frequency, making it unsuitable for fixed band communication purposes. To the best of our knowledge, no work has been done so far to implement a microwave sensor with other microwave components in the same substrate having a common input port.

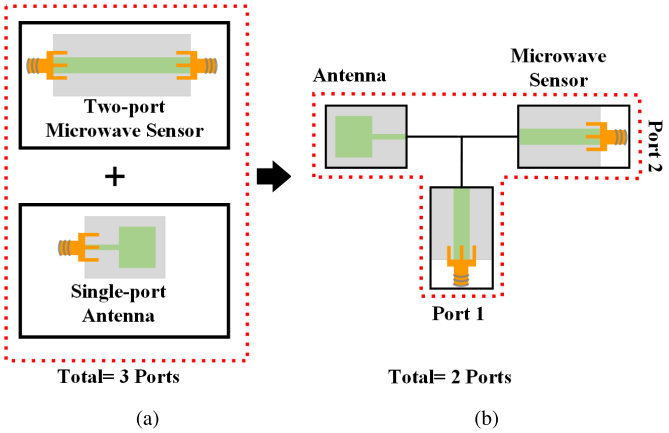

Fig. 1. Ports requirement of (a) separate microwave sensor and antenna in a single substrate (b) our proposed design.

In this article, we propose a novel concept of integrating a microwave sensor with a communicating antenna using a novel frequency-selective multipath filter (FSMF) in the same substrate ($\epsilon_r = 3.55$, $\tan\delta = 0.0027$, and thickness of 0.81 mm) having a common input source. The proposed design provides a solution to several problems mentioned in the following.

1) It reduces the total number of required ports of a multifunctional microwave sensing system from 3 to 2, as shown in Fig. 1. For example, if a microwave sensor and an antenna are placed separately on a single

substrate, two ports for the microwave sensor and at least a single port for the antenna are required. In total, three ports are needed. We have achieved the same functionality with only two ports in our proposed design, thus reducing the required hardware components.

2) Integration of multifunctional devices reduces the overall size of a system. In addition, a complete planar structure eliminates unintentional reflections, which may occur if two separate microwave components are joined together.
3) Due to the presence of the FSMF, the frequency shift of the microwave sensor in the presence of different MUTs does not alter (or affect) the operational bandwidth of the communication antenna.
4) Unlike the existing works mentioned above, our proposed microwave sensor measures one additional sensing parameter, i.e., the frequency distance of two closely spaced resonance frequencies of the microwave sensor in the presence of an MUT. Thus, it has a higher degree of freedom for material characterization.

To summarize, the main novelty of our proposed design is to use multifunctional microwave devices in the same substrate having a common input source without affecting each other's performance. Furthermore, the additional sensing parameter of the microwave sensor can enhance the sensing capabilities of the sensor.

The rest of the manuscript is organized as follows. Section II discusses the novel aspects of the proposed solution and design overview. The design details of the FSMF, microwave sensor, and antenna are provided in Sections III, and IV, respectively. The integration of the FSMF, antenna, and microwave sensor is given in Section V. Section VI presents the measurement results and discussions. Finally, this article is concluded in Section VII.

II. Design Overview

The main idea behind our proposed design is to integrate two separate microwave components for different applications. In this article, we have designed an antenna for wireless application at 2.45 GHz and a microwave sensor for sensing application. The sensing capability of the microwave sensor is demonstrated using different concentrations of water–gasoline and ethanol–gasoline mixtures. However, the concept can also be applied for sensing other analytes utilizing appropriate sensing materials. The multifunctional devices have been integrated with the FSMF. The design of the FSMF is very crucial. The FSMF has two different paths at its output. A high-pass filter (HPF) (with cutoff frequency $f_c = 3.5$ GHz) has been integrated at path 1 of the FSMF. Similarly, a low-pass filter (LPF) (with cutoff frequency, $f_c = 2.85$ GHz) has been integrated at path 2 of the FSMF. The microwave sensor is included at port 2 of the FSMF, and the fixed band antenna is connected at port 3 of the FSMF. Similarly, as the antenna will be connected before the LPF, it will not affect the performance of the microwave sensor (see Fig. 2).

To ensure that the designed LPF does not affect the performance of the HPF, the insertion loss of the LPF beyond the cutoff frequency of the HPF has been made very high. Similarly, the insertion loss of HPF below the cutoff frequency of the LPF has been made significant for the same reason. The block diagram of the entire design is shown in Fig. 2.

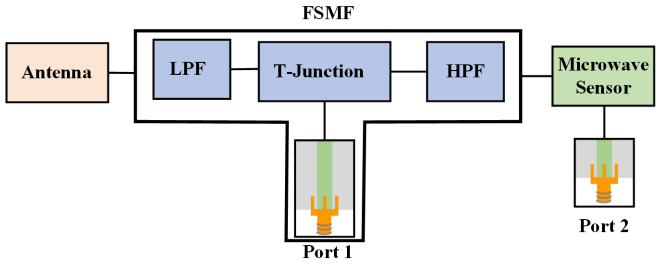

Fig. 2. Block diagram of the proposed multifunctional system.

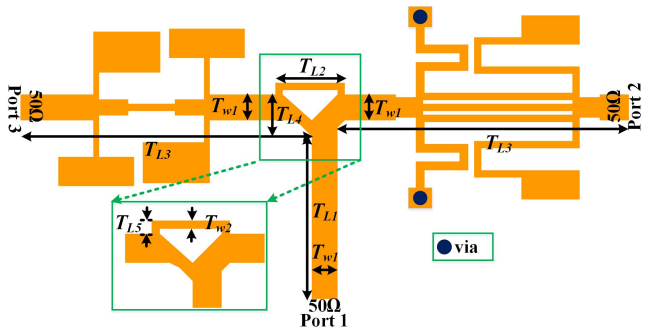

Fig. 3. Proposed FSMF. Here, $T_{W1} = 1.77$, $T_{W2} = 0.5$, $T_{L1} = 11.1$, $T_{L2} = 4.8$, $T_{L3} = 20$, $T_{L4} = 2.9$, and $T_{L5} = 0.8$ (all in mm).

III. Frequency-Selective Multipath Filter

We aim to design a multifunctional microwave system in the same substrate using the same input source while maintaining the system's compactness. Furthermore, to integrate the microwave devices and ensure that they have minimum effect on each other's performance, an FSMF is proposed, as shown in Fig. 3. The FSMF is designed by integrating an LPF filter and an HPF filter on two different paths of a modified T-junction. The combination of LPF-HPF is chosen to ensure independent operations of the communication antenna and the microwave sensor at 2.45 GHz and over 4–6 GHz, respectively.

The electric field perturbation of the microwave sensor in the presence of different MUT will shift its resonance frequency. Hence, connecting the microwave sensor to the output port of the HPF will limit the frequency shift till the cutoff frequency of the HPF, ensuring no impact on the performance of the communicating antenna. Choosing a combination of LPF-HPF with nonoverlapping frequencies can, thus, create a proper condition for multifunctional operations. In the following, a detailed description of the design and performance of the LPF and HPF filters and their integration in the FSMF, are given separately in the following.

A. Design of the LPF and HPF

A communicating antenna will be connected at port 3 of the FSMF, i.e., the output port of the LPF. Therefore, the LPF filter has been designed such that it passes the signal

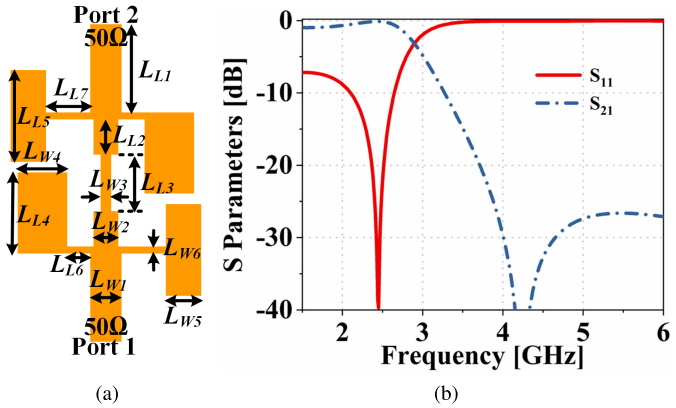

Fig. 4. Proposed (a) LPF and (b) S-parameters of the LPF. Here, $L_{W1} = 1.77$, $L_{W2} = 1.4$, $L_{W3} = 0.6$, $L_{W4} = 2.8$, $L_{w4} = 2.8$, $L_{W5} = 2$, $L_{W6} = 0.4$, $L_{L1} = 5$, $L_{L2} = 2$, $L_{L3} = 3.2$, $L_{L4} = 4.6$, $L_{L5} = 5.2$, $L_{L6} = 1.3$, and $L_{L7} = 2.5$ (all in mm).

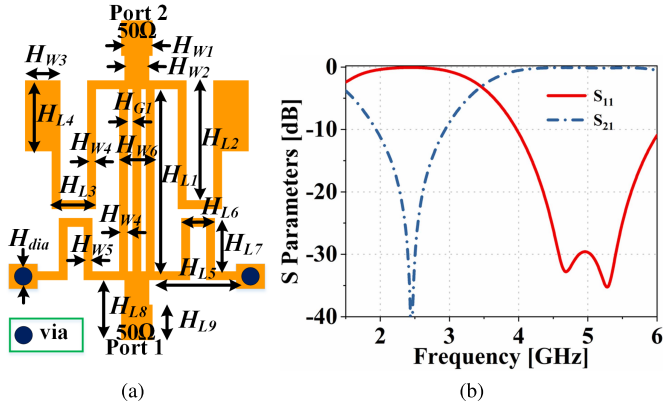

Fig. 5. Proposed (a) HPF and (b) S-parameters of the HPF. Here, $H_{W1} = 1.77$, $H_{W2} = 1.4$, $H_{W3} = 2$, $H_{W4} = 0.5$, $H_{w5} = 0.5$, $H_{W6} = 2$, $H_{L1} = 10.3$, $H_{L2} = 6.8$, $H_{L3} = 2.5$, $H_{L4} = 4$, $H_{L5} = 4.9$, $H_{L6} = 1.9$, $H_{L7} = 3$, $H_{L8} = 3.8$, $H_{L9} = 2$, $H_{G1} = 0.25$, and $H_{\text{dia}} = 1$ (all in mm).

below 2.85 GHz. Furthermore, as the LPF and the HPF are connected to the FSMF, it is important to mention that the LPF should have a very high insertion loss at the operation region of the HPF, i.e., between the 3.5- and 6-GHz frequency range. Fig. 4(a) shows the layout of the proposed LPF. The LPF is designed by following the methodology proposed in [34], [35], and [36]. The LPF consists of a step-impedance-based main feedline together with open-ended shunt stubs. The designed filter has very good matching and low insertion loss at 2.45 GHz. The S_{11} and S_{21} responses of the filter, as shown in Fig. 4(b), confirm this.

Similarly, a microwave sensor will be connected at port 2 of the FSMF, i.e., the output port of the HPF. Consequently, the HPF is designed such that it passes frequencies over 4 GHz. Furthermore, as this filter and the LPF are connected to the FSMF, the insertion loss of this filter must be very high where the LPF will be operating, i.e., between the 2- and 3-GHz frequency range. The layout of the HPF is shown in Fig. 5(a). The HPF is designed by following the methodology proposed in [36], [37], and [38]. The layout of the HPF includes two long slots on the feedline. The total equivalent coupling capacitance of the slots acts in series with the main feed line. Two shorted-end microstrip lines are connected on one side of the feedline. The lines have equal impedances. The equivalent inductances of the line are in shunt with the main feed line. On the other side of the feedline, two open-ended microstrip lines are connected in a shunt. The S-parameters of the proposed HPF are shown in Fig. 5(b).

B. Integration of LPF and HPF in FSMF

Finally, the LPF and the HPF are connected with a modified T-junction. The junction of the microstrip feed is designed to retain the individual characteristics of the filters by providing maximum matching to the LPF and the HPF at 2–3 and 4–6 GHz frequency bands, respectively. Integration of the components shifted the operational frequency band of the LPF. Therefore, the design parameters of the LPF are optimized again to provide maximum matching at 2.45 GHz ($L_{W2} = 1.1$, $L_{W3} = 0.5$, and $L_{L6} = 1.5$). In addition, some design parameters of the HPF ($H_{W5} = 0.6$, $H_{L1} = 10.2$, $H_{L5} = 4.7$, and $H_{L6} = 1.8$) are also reoptimized to provide maximum matching near about 5 GHz. Integrating the LPF and HPF on the two different paths of the FSMF reduces the individual matching of both the filters over their operating frequency bands. The matching reduction makes port 3 of the FSMF output a bandpass filter instead of an LPF, as shown in Fig. 6.

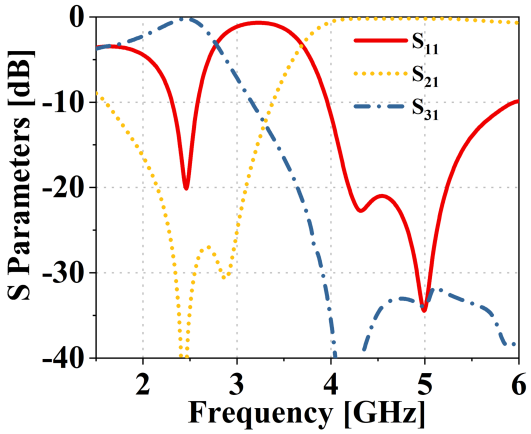

Fig. 6. S-parameters of FSMF.

From Fig. 3, it is visible that port 2 and port 3 of the FSMF are the output of HPF and LPF, with cutoff frequencies at 3.5 and 2.85 GHz, respectively. Furthermore, the S_{31} and S_{21} responses (as shown in Fig. 6) of the FSMF confirm that these two-output ports are acting as an output port of an LPF and an HPF.

The FSMF integrates two multifunctional devices that operate over nonoverlapping frequency spectrums. The FSMF has a 50 Ω input impedance, and the impedance of the output ports also has been kept at 50 Ω to ensure minimum reflection on integrating a 50 Ω microwave sensor and an antenna with a 50 Ω feedline.

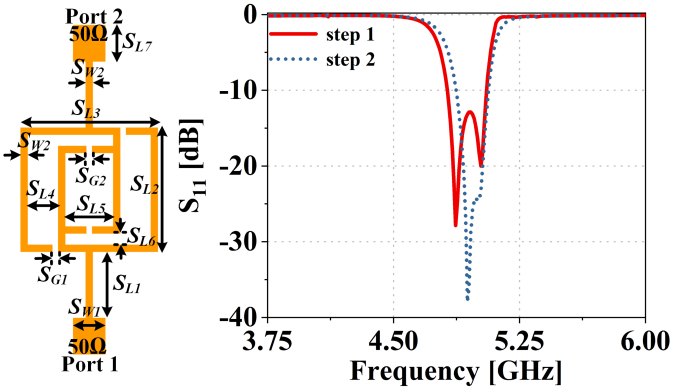

Fig. 7. Proposed (a) microwave sensor and its (b) input reflection coefficient at $S_{L5} = 2.7$ (step 1) and $S_{L5} = 2.6$ (step 2). Here, $S_{W1} = 1.77$, $S_{W2} = 0.4$, $S_{L1} = 3.6$, $S_{L2} = 6.8$, $S_{L3} = 7.5$, $S_{L4} = 1.65$, $S_{L5} = 2.6$, $S_{L6} = 0.6$, $S_{L7} = 2$, $S_{G1} = 0.2$, and $S_{G2} = 0.2$ (all in mm).

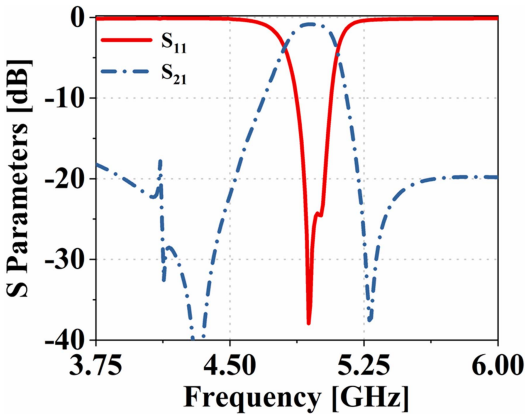

Fig. 8. S-parameter responses of the microwave sensor.

IV. Microwave Sensor and Antenna Design

A. Design of Microwave Sensor

As mentioned in Section I, microwave sensors have been primarily designed to observe changes in resonance frequency and/or transmission coefficient. In addition to that, the design objective of our proposed microwave sensor is to provide one additional sensing parameter. This additional parameter is the frequency distance between two closely spaced resonance frequencies. The main feedline of the microwave sensor has been designed to provide a 50 Ω impedance to ensure minimum reflection on integration with port 2 of FSMF. The dimensions of the proposed sensor are shown in Fig. 7(a). The microwave sensor resonates at two distinct frequencies. The separation between these frequencies is reduced by changing the parameter S_{L5}. Finally, at $S_{L5} = 2.6$ mm, both the resonance frequencies come very closer to each other and make the microwave sensor's operating frequency from 4.5 to 4.7 GHz, as shown in Fig. 7(b). The S_{L5} parameter value is chosen to make the two distinct resonance frequencies visible. The S-parameters of the designed microwave sensor are shown in Fig. 8. The S-parameters in the presence of MUTs (from $\epsilon_r = 2$ to 20) are shown in Fig. 9. The frequency separation of

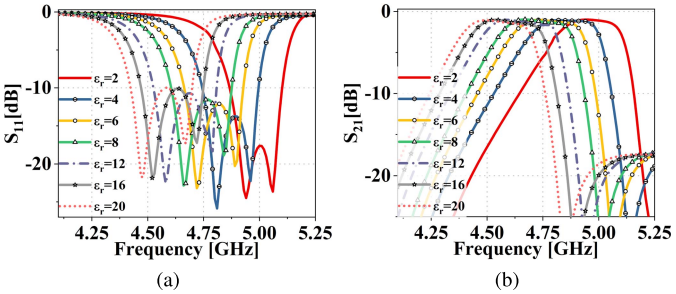

Fig. 9. Simulated (a) S_{11} and (b) S_{21} responses of the microwave sensor in the presence of different MUTs.

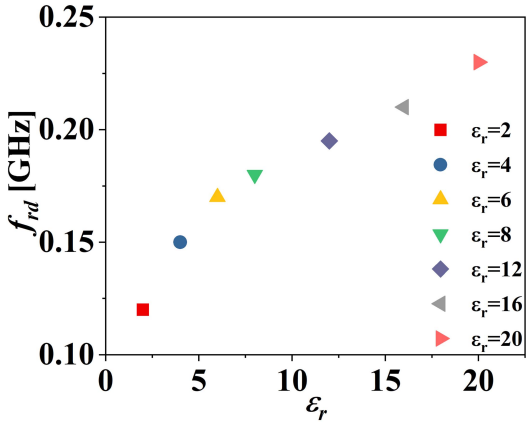

Fig. 10. Differences between two closely spaced resonance frequencies in the presence of different MUTs.

two closely spaced resonance frequencies with changes in the relative permittivity of the MUTs is shown in Fig. 10, where

$$f_{rd} = f_{r1} - f_{r2}. \tag{1}$$

The container of the MUT is given the attributes of 3-D printing material polylactic acid (PLA), i.e., $\epsilon_r = 2.6$ and $\tan\delta = 0.025$. The material properties of the empty holder on top of the resonator preshift the resonance frequencies of the microwave sensor; thus, the sensor needs to be optimized again to detect MUTs with higher permittivity within the desired frequency range. From Fig. 10, it is visible that changing the material properties of the liquid not only shifts the resonance frequencies and transmission coefficient but also increases the distance between two jointly spaced resonance modes. The electric field plot from Fig. 11 shows a high electric field concentration near g1 and g2 for the first and second resonance modes, respectively. An MUT on top of the sensor perturbs the electric field. The interaction of the electric field with the MUT changes the resonance frequency. Different electric field strengths of gap g1 (at resonance mode 1) and g2 (at resonance mode 2) shift the resonance frequencies differently for different MUTs. These shifts in the resonance frequencies can be defined by [39]

$$\Delta f_{r1} = -f_r\left(\frac{\epsilon_{\text{MUT}} - 1}{2}\right)\left(\frac{\int_{V_s} E \cdot E_1 dV}{\int_{V_c} |E_1|^2 dV}\right) \tag{2}$$

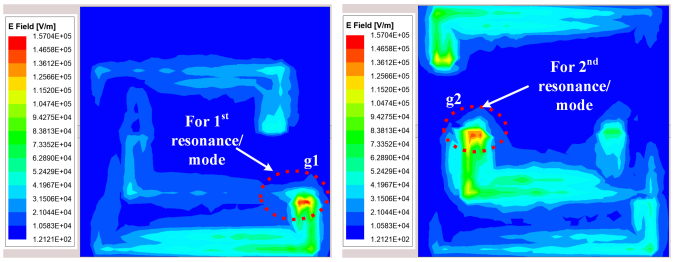

Fig. 11. Electric-field distribution of the microwave sensor at (a) first resonant mode and (b) second resonant mode.

$$\Delta f_{r2} = -f_r\left(\frac{\epsilon_{\text{MUT}} - 1}{2}\right)\left(\frac{\int_{V_s} E \cdot E_2 dV}{\int_{V_c} |E_2|^2 dV}\right) \tag{3}$$

where Δf_{r1} is the shift of the first resonance frequency mode in the presence of an MUT and Δf_{r2} is the shift of the second resonance frequency mode in the presence of the same MUT. E is the electric field of the bare sensor (without MUT), E_1 is the electric field strength of the first resonance mode, and E_2 is the electric field strength of the second resonance mode. Hence, if $f_{r2} > f_{r1}$, then the distance between two closely spaced resonance frequencies is defined as

$$\Delta f_{r1} - \Delta f_{r2}. \tag{4}$$

B. Antenna Design

As mentioned above, the antenna for communication purposes will be connected to the output port of the LPF, i.e., in port 3 of the FSMF. The antenna's feedline has been designed for 50 Ω impedance to minimize the reflection on integration with the FSMF. Therefore, the width of the antenna feedline is the same as the width of port 3 of FSMF. Also, the ground plane of the FSMF and the microwave sensor will remain on the back of the system. Thus, it will also act as a ground plane for the proposed antenna. The proposed antenna and its input reflection coefficient are shown in Figs. 12 and 13.

The antenna has been designed for Wi-Fi applications at 2.45 GHz. The proposed antenna has a −10 dB impedance bandwidth that goes from 2.28 to 2.69 GHz. Therefore, integrating the FSMF filter on the antenna's feedline chooses only the desired bandwidth at 2.45 GHz out of the broad spectrum. The radiation patterns of the antenna in two orthogonal planes are shown in Fig. 13.

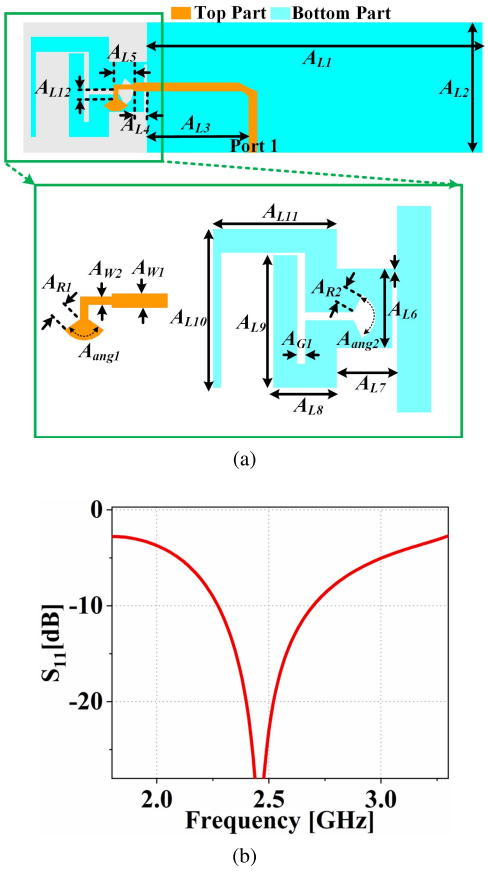

Fig. 12. (a) Proposed antenna for Wi-Fi applications and (b) its input reflection coefficient. Here, $A_{W1} = 1.77$, $A_{W2} = 1$, $A_{L1} = 67.1$, $A_{L2} = 26$, $A_{L3} = 20.3$, $A_{L4} = 2.7$, $A_{L5} = 4$, $A_{L6} = 10$, $A_{L7} = 7.6$, $A_{L8} = 8$, $A_{L9} = 16.7$, $A_{L10} = 20$, $A_{L11} = 15.6$, $A_{L12} = 1.85$, $A_{R1} = 2.4$, $A_{R2} = 2.5$, and $A_{G1} = 1$ (all in mm), and $A_{\text{ang1}} = 110°$ and $A_{\text{ang2}} = 130°$.

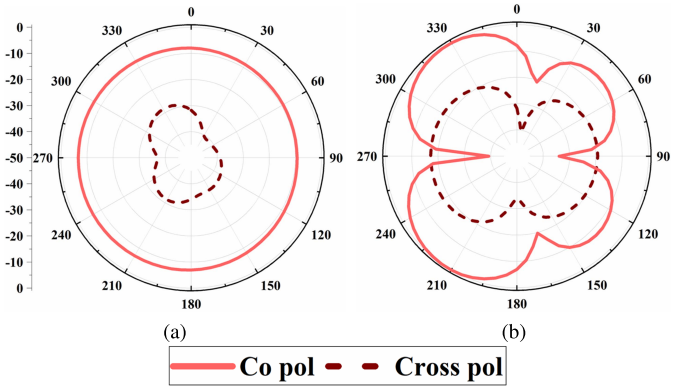

Fig. 13. Simulated radiation pattern of the antenna at 2.45 GHz in (a) E-plane and (b) H-plane.

V. Integration of All the Components and Modeling of Different Mixtures

Finally, the antenna, FSMF, and the microwave sensor are connected together, as shown in Fig. 14(a). The simplified lumped element equivalent circuit of the integrated dual-functional system is represented in Fig. 14(b), where L_{T1} and L_{T2} represent the inductance associated with the T-junction, while C_{T1} represents the cumulative capacitances associated with the T-junction discontinuity. L_P, C_P, and L_H, C_H represent the inductances and capacitances associated with the LPF and HPF, respectively. The RLC tank circuit represents the resonance frequency of the communicating antenna. Inductances and capacitances associated with the microwave sensor are represented by L_S and C_S. After integration, the reoptimized design parameters of the proposed system are $L_{W2} = 0.6$, $L_{W3} = 0.4$, $H_{W5} = 0.6$, $H_{L1} = 10.15$, $H_{L5} = 4.7$, $H_{L6} = 1.8$, $S_{L1} = 4.35$, $S_{L2} = 6.75$, $S_{L4} = 1.7$, $S_{L5} = 2.5$, and $S_{L7} = 4.8$. The simulated input reflection

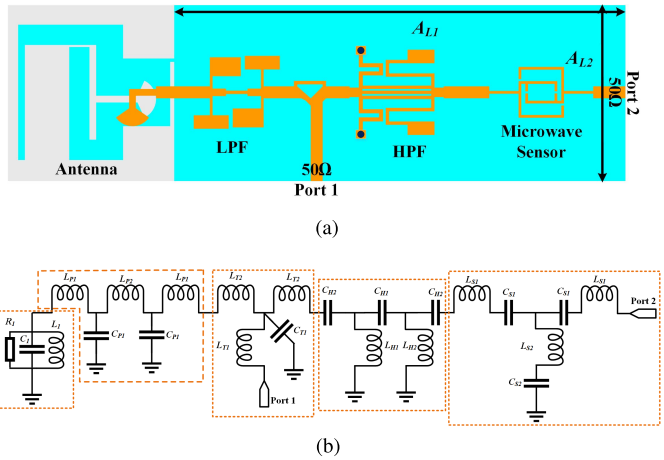

Fig. 14. (a) Proposed dual-functional system. (b) Equivalent circuit of the proposed system.

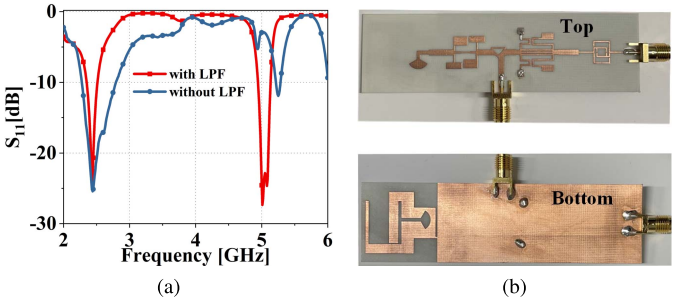

Fig. 15. (a) Simulated input reflection coefficient of the proposed dual-functional system with and without the LPF. (b) Fabricated view of the proposed system.

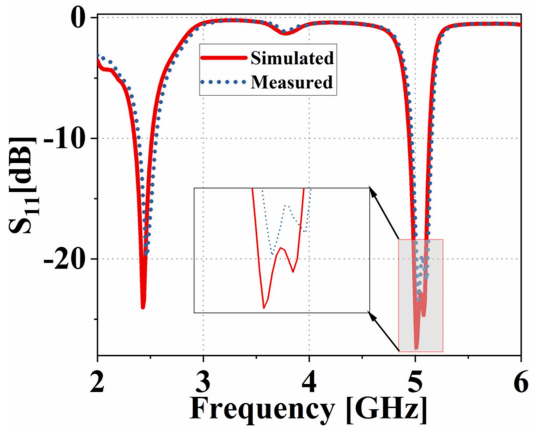

Fig. 16. Input reflection coefficient of the proposed system.

coefficients of the proposed dual-functional system with and without the LPF are shown in Fig. 15(a). In the absence of the LPF, the input reflection coefficient of the antenna beyond the cutoff frequency of the LPF affects the input reflection coefficient of the sensor at port 1, leading to poor matching of both the closely spaced resonance frequencies of the sensor at 5 GHz. The top and bottom views of the proposed system are presented in Fig. 15(b). The simulated and measured S_{11} and S_{21} of the proposed system are shown in Figs. 16 and 17(a). The simulated radiation efficiency

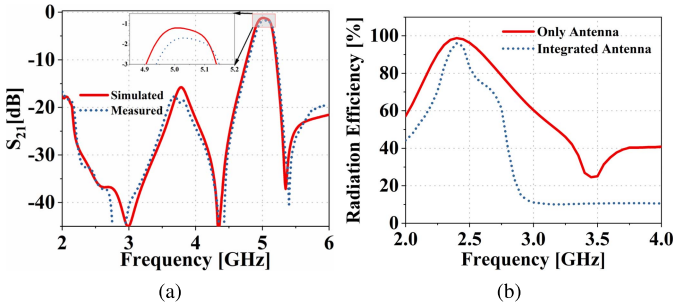

Fig. 17. (a) Transmission coefficient of the proposed system and (b) radiation efficiency of the communication antenna before and after integration with the complete design.

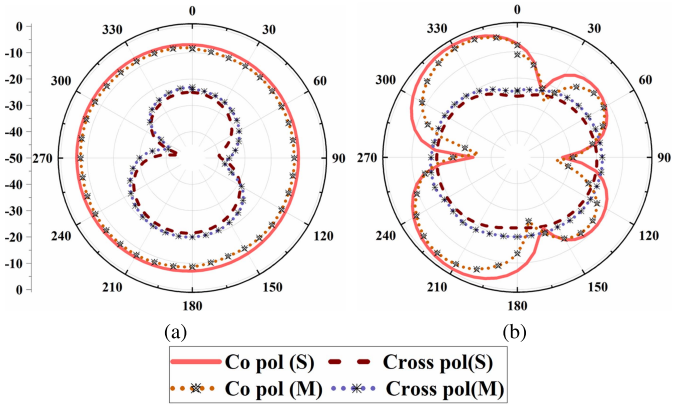

Fig. 18. Simulated and measured radiation patterns of the proposed system at 2.45 GHz in (a) E-plane and (b) H-plane.

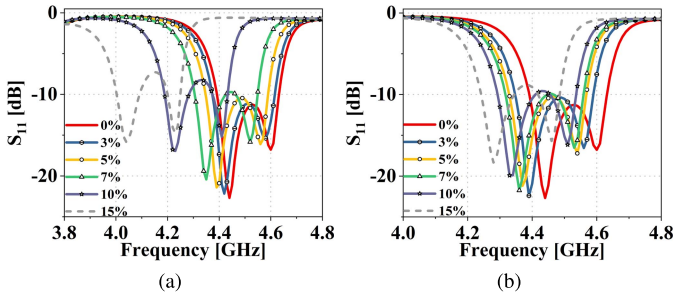

Fig. 19. Simulated input reflection coefficients (directly on top, in a PLA container without bottom surface) for 0%–15% concentrations of (a) water–gasoline and (b) ethanol–gasoline mixtures.

of the communicating antenna before and after integration with the FSMF is shown in Fig. 17(b). After integrating with the FSMF, the radiation efficiency of the antenna at 2.45 GHz gets reduced due to the insertion loss of the LPF of the FSMF. Also, from Fig. 17(b), it is visible that the radiation efficiency of the proposed system has almost become negligible beyond the cutoff frequency of the LPF. This shows that the LPF of the FSMF chooses only the desired bandwidth at 2.45 GHz, filtering the remaining frequency spectrum for fixed band communication. The measured radiation efficiency of the antenna is above 80% (89% at 2.45 GHz) throughout the operating bandwidth of the communicating antenna. The measured maximum gain of the communicating antenna at

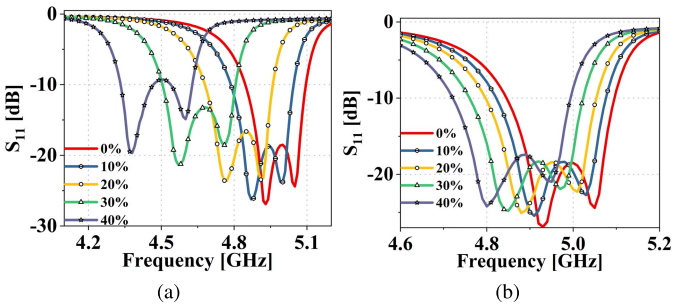

Fig. 20. Simulated input reflection coefficients (in a PLA container with the bottom surface) for 0%–40% concentrations of (a) water–gasoline and (b) ethanol–gasoline mixtures.

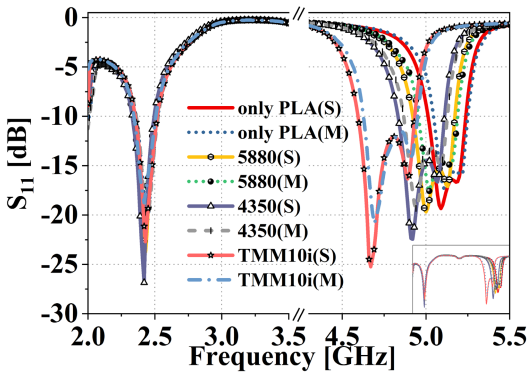

Fig. 21. Simulated and measured input reflection coefficients of the proposed system in the presence of different PCB blocks on top of the PLA slab attached to the microwave sensor.

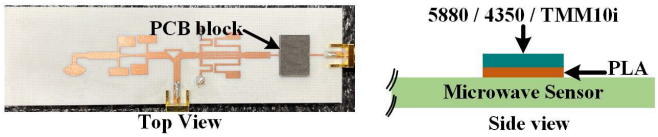

Fig. 22. Validation arrangement of the proposed system.

2.45 GHz is 4.9 dBi. The simulated and measured radiation patterns of the communicating antenna at 2.45 GHz in both orthogonal planes after integrating with the complete system are shown in Fig. 18. Comparing Figs. 13 and 18, it is visible that the copolarization remains very similar to each other. This confirms the absence of unintentional radiations from other components of the complete system at 2.45 GHz.

A. Modeling of Water–Gasoline and Ethanol–Gasoline Mixtures

Before directly measuring the mixtures using the microwave sensor, different models are created for water–gasoline and ethanol–gasoline mixtures.

In practice, it is impossible for water and gasoline to get into a single state; hence, for modeling water–gasoline mixtures, series–parallel (SP) is widely used. According to the SP model, the permittivity of the mixture with different concentrations can be calculated using

$$\epsilon_{\text{MUT}} = \eta\left(\alpha\epsilon_{\text{water}} + (1-\alpha)\epsilon_{\text{gasoline}}\right) + (1-\eta)\epsilon_{\text{water}}\epsilon_{\text{gasoline}}\left(\alpha\epsilon_{\text{gasoline}} + (1-\alpha)\epsilon_{\text{water}}\right)^{-1} \quad (5)$$

$$\eta = 2\alpha(5-3\alpha)^{-1} \quad (6)$$

where α is the mixing ratio and η is the polarization state. The complex permittivity of water, gasoline, and ethanol [40], [41], [42] at room temperature in the frequency range of 4–5 GHz is available in the literature.

On the other hand, ethanol can be easily blended with gasoline. Therefore, the ethanol–gasoline mixture is modeled using the Maxwell–Garnett (MG) [43] formula. The MG formula is used to find the effective permittivity of ethanol mixtures [44]. According to the MG formula, the permittivity of the mixture with different concentrations can be calculated using [42]

$$\epsilon_{\text{MUT2}} = \epsilon_{\text{gasoline}} + 3\alpha\epsilon_{\text{gasoline}} \times \left(\frac{\epsilon_{\text{ethanol}} - \epsilon_{\text{gasoline}}}{\epsilon_{\text{ethanol}} + 2\epsilon_{\text{gasoline}} - \alpha\left(\epsilon_{\text{ethanol}} - \epsilon_{\text{gasoline}}\right)}\right). \quad (7)$$

The simulated input reflection coefficients for 0%–15% and 0%–40% concentrations of water–gasoline and ethanol–gasoline mixtures are represented in Figs. 19 and 20.

VI. Measurements and Discussion

The main objective of the proposed system is to show multifunctional operation without affecting the operational bandwidth of the communicating antenna in the presence of different MUTs on top of the microwave sensor. This is first shown in the validation of the proposed system, as mentioned in the following.

A. Validation of the Proposed System

The proposed system is first validated using PCB substrates with different dielectric constants. To validate the model, PCB blocks (after removing the copper on both sides) of 10.5 × 8.5 mm^2 size are prepared from Rogers RT Duroid 5880 (0.78 mm), Rogers 4350 (0.76 mm), and Rogers TMM10i (0.76 mm) substrates. The PCB blocks have some standard thickness. However, for a fair comparison, the PCB blocks are chosen in such a way that they have a similar thickness. These PCBs have a dielectric constant of 2.2–9.8. To consider the effect of the bottom wall of the 3-D printed PLA container (mentioned in Section VI-B), a PLA slab of dimension 10.5 × 8.5 × 0.6 mm^3 is also prepared. The proposed system's input reflection coefficient for each measurement is shown in Fig. 21. The measurements are taken by first placing the PLA slab on top of the sensor and then placing all the PCB blocks on top of the PLA slab, as shown in Fig. 22. The figure shows that, despite the presence of PCB blocks of different dielectric constants on top of the sensor, the −10 dB impedance bandwidth of the communicating antenna remains almost constant for all the measurements. The simulated and measured results are in good agreement. This validates our proposed system. Fig. 23 shows the simulated and measured frequency distances of the two closely spaced resonance frequencies of the microwave sensor

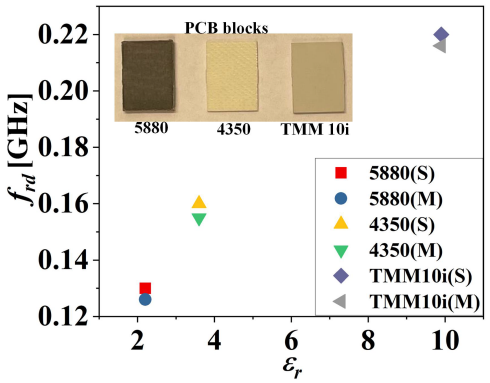

Fig. 23. ϵ_r of the PCB blocks versus frequency distance of the two closely spaced resonance frequencies of the microwave sensor in the presence of each PCB block on top of the PLA slab.

in the presence of each PCB block on top of the PLA slab, which is attached to the microwave sensor.

B. Measurements of Different Water–Gasoline and Ethanol–Gasoline Mixtures

The proposed microwave sensor also characterizes different concentrations of water–gasoline and ethanol–gasoline mixtures. The mixtures are characterized by two diverse ranges of concentrations, i.e., 0%–15% and 0%–40%. The volume of the liquid ($10.5 \times 8 \times 4$ mm^3) is kept the same for both cases. For 0%–15% concentration, the MUT mixtures are directly applied to the sensor inside a 3-D printed PLA holder. In this case, the PLA holder does not have any bottom wall, and the holder is attached to the substrate using silicone glue, while, for 0%–40% concentrations, a 3-D printed PLA holder with a bottom wall of 60 μm thickness is used. As in this case, the empty container lies directly on top of the resonator, and it preshifts the resonance frequencies of the microwave sensor; thus, some design parameters of the sensor are optimized again ($S_{L1} = 4.85$, $S_{L2} = 5.55$, $S_{L4} = 1.7$, and $S_{L5} = 2.45$) to detect MUTs with higher permittivity within the desired frequency range. This means that the liquid and the sensor are separated by a distance of 60 μm for the second case. An increment of the concentration of water or ethanol in gasoline also increases the permittivity of the mixture. The direct application of the mixture on top of the sensor increases its sensitivity. Therefore, the MUT is directly applied to the sensor to distinguish minor changes in the mixture permittivity in the 0%–15% concentration range. On the other hand, for 0%–40% mixture concentration measurement, a 3-D printed PLA container with a bottom wall is used. Direct application of the liquid (with high mixture concentrations) on top of the sensor reduces its lifetime; hence, using a 3-D printed container can be an efficient choice at the cost of lesser sensitivity. The dimensions of the PLA containers are shown in Fig. 24. Various samples are prepared to measure different mixtures, as shown in Fig. 25. The measured input reflection coefficients for 0%–15% concentrations (directly on top, in a PLA container without a bottom surface) and 0%–40% concentrations of water–gasoline and ethanol–gasoline mixtures are represented in Figs. 26 and 27. The measurement

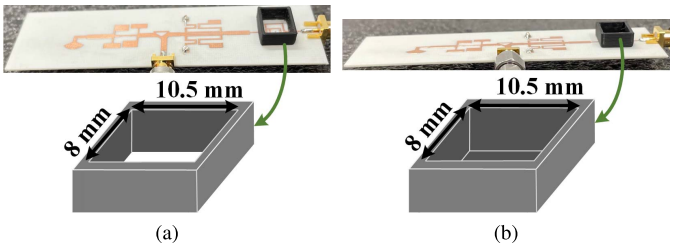

Fig. 24. PLA container for (a) 0%–15% (without bottom wall) and (b) 0%–40% (with bottom wall).

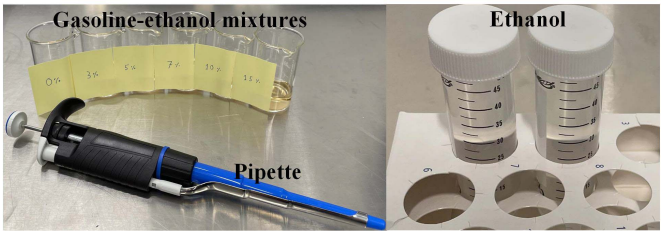

Fig. 25. Prepared samples.

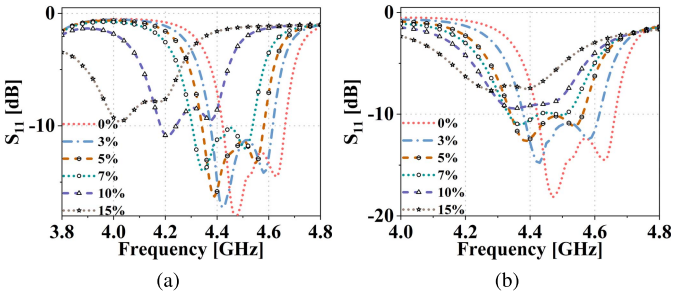

Fig. 26. Measured input reflection coefficients (directly on top, in a PLA container without bottom surface) for 0%–15% concentrations of (a) water–gasoline and (b) ethanol–gasoline mixtures.

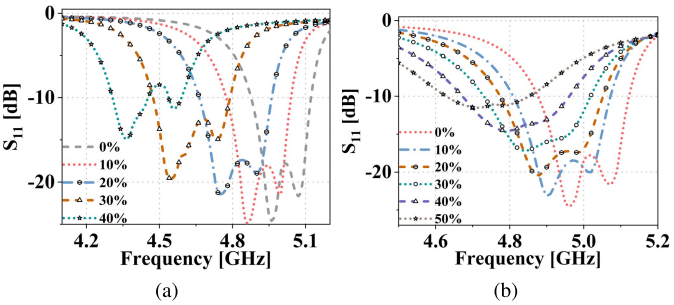

Fig. 27. Measured input reflection coefficients (in a PLA container with the bottom surface) for 0%–40% concentrations of (a) water–gasoline and (b) ethanol–gasoline mixtures.

shows a shift in resonance frequency with increasing concentration for both cases, as shown in the simulated results presented in Figs. 19 and 20. However, the y-axis levels of the input reflection coefficient are slightly different from the simulated results, which could be due to the purity of liquids and the loss tangent of the mixtures. Nevertheless, the frequency shift of the model seems in good agreement with the measurement results. Furthermore, the two resonance

TABLE II
DIELECTRIC CHARACTERIZATION USING EXISTING MICROWAVE SENSORS

Ref.	Measured parameters	$\epsilon_r = f(a,b)$	f_0 (without MUT) [GHz]	Sensor size [mm^3]
[26]	$\Delta f_0, S_{21}$	$f(\Delta f_0, \Delta\lvert S_{21}\rvert)$	~1.9	N/A
[30]	$\Delta f_0, S_{21}$	$f(\Delta f_0, \Delta\lvert S_{21}\rvert)$	2.226	35×20×0.76
[44]	$\Delta\phi, \Delta mag$	$f(\Delta\phi, \Delta mag)$	N/A	[a]156×41×0.8
[45]	$\Delta\phi, \Delta mag$	$f(\Delta\phi, \Delta mag)$	N/A	61×48×0.338
[46]	$\Delta f_0, \Delta Q$	$f(\Delta f_0, \Delta Q)$	~2.4	28×20×0.75
[47]	S_{21}	N/A	5.8	N/A
[16]	$S_{21}, \Delta f_0$	$f(\Delta f_0)$	3.75	N/A
[48]	$\Delta f_0, \Delta Q$	$f(\Delta f_0, \Delta Q)$	2.637	~78×65×6.1
[49]	$S_{21}, \Delta f_0$	N/A	1.6	N/A
*TW	$\Delta f_{c0}, \Delta f_{rd}, S_{21}$	$f(\Delta f_{c0}, \Delta f_{rd})$	[b]5.03, [c]5.11	25×26×0.81

[a]Including the distance between transmitting/receiving antenna; [b]first RSF; [c]second RSF.

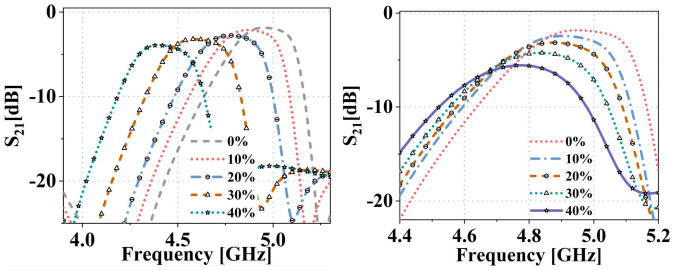

Fig. 28. Measured transmission coefficients for 0%–40% concentrations of (a) water–gasoline and (b) ethanol–gasoline mixtures.

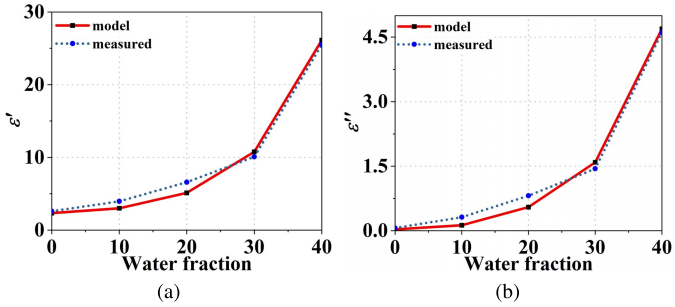

Fig. 29. Comparison between the model and measured values of 0%–40% water–gasoline mixtures. (a) Real and (b) imaginary parts of the complex permittivity.

frequencies get blurred into one beyond 7% in Fig. 26(b) and beyond 30% in Fig. 27(b), mainly due to ethanol's high loss tangent (approximately 0.80). Hence, using the proposed parameter, the characterization of ethanol–gasoline mixtures can be done up to 30%. The measured transmission coefficients of 0%–40% water–gasoline and ethanol–gasoline mixtures are shown in Fig. 28.

In the literature, as shown in Table II, the input reflection and transmission coefficients of a two-port microwave device are used for the detection and dielectric characterization of different MUTs. In [26] and [30], the complex permittivity of different MUTs is expressed in terms of resonance frequency shift (Δf_0) and change in transmission coefficient. In [44] and [45], the phase and magnitude of transmission coefficient are used for the characterization of different MUTs.

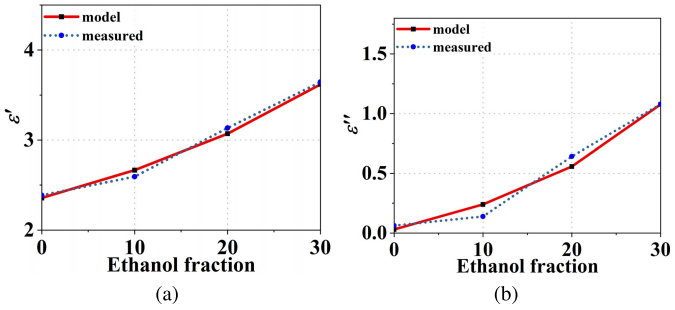

Fig. 30. Comparison between the model and measured values of 0%–30% ethanol–gasoline mixtures. (a) Real and (b) imaginary parts of the complex permittivity.

On the other hand, in [46] and [48], Δf_0 and change in the quality factor (Q) is used to characterize different MUTs. The quality factor is also a function of resonance frequency and -3 dB bandwidth (S_{21}). In [16], only the real part of permittivity is expressed as a function of Δf_0. In [47] and [49], ethanol/water mixtures and acetone/water mixtures are sensed, respectively, but their dielectric properties are not characterized.

In our proposed design, we have characterized the MUTs in terms of $f(\Delta f_{c0}, \Delta f_{\text{rd}})$, where f_{c0} denotes the center frequency of the input reflection coefficient (-10 dB bandwidth), and f_{rd} is the frequency distance of two closely spaced resonance frequencies. That means that our proposed parameter can be used as an alternative to transmission coefficient or can be used as an additional parameter giving more degree of freedom. The characterization of different MUTs for 0%–40% water–gasoline mixtures can be derived [30] as

$$\begin{bmatrix} \Delta\epsilon' \\ \Delta\epsilon'' \end{bmatrix} = \begin{bmatrix} -149.8810 & -588.1196 \\ -30.6205 & -122.0545 \end{bmatrix} \begin{bmatrix} \Delta f_{c0} \\ \Delta f_{\text{rd}} \end{bmatrix} \tag{8}$$

where $\Delta f_{c0} = f_{c0}^{\text{mut}} - f_{c0}^{\text{ref}}$, $\Delta f_{\text{rd}} = f_{\text{rd}}^{\text{mut}} - f_{rd}^{\text{ref}}$, $\Delta\epsilon' = \epsilon'_{\text{mut}} - \epsilon'_{\text{ref}}$, $\Delta\epsilon'' = \epsilon''_{\text{mut}} - \epsilon''_{\text{ref}}$, and "ref" denotes gasoline. Using the same method, the characterization of different MUTs for 0%–30% ethanol–gasoline mixtures can be done as

$$\begin{bmatrix} \Delta\epsilon' \\ \Delta\epsilon'' \end{bmatrix} = \begin{bmatrix} 10.1277 & -168.8476 \\ 13.1299 & -179.3756 \end{bmatrix} \begin{bmatrix} \Delta f_{c0} \\ \Delta f_{\text{rd}} \end{bmatrix}. \tag{9}$$

A comparison of the complex permittivity of the model (as mentioned in Section V-A) and the measured values of MUTs are shown in Figs. 29 and 30.

VII. Conclusion

A dual-functional microwave system with a novel FSMF is presented in this article. The FSMF allows fixed band operation of the communicating antenna without affecting its operational bandwidth in the presence of different MUTs on top of the sensor. The proposed design shows an efficient integration of a microwave sensor with a communicating antenna without affecting each other's performance. The ability of FSMF to combine two different microwave components could also be utilized for several other microwave applications. Furthermore, the proposed microwave sensor has the unique functionality of measuring one additional parameter, which is the frequency distance of two closely spaced resonance frequencies in the presence of different MUTs. The additional sensing parameter of the sensor can enhance the capability of a microwave sensor for better characterization of different materials. The model is validated using different standard PCB blocks, which shows good agreement with the simulated results. The microwave sensor also shows that it can perform characterization of water–gasoline and ethanol–gasoline mixtures for 0%–40% and 0%–30% concentrations. By adjusting the design parameters, the proposed concept can also be applied for antenna applications at other frequencies and sensors (utilizing appropriate sensing materials) for sensing other liquid and gas analytes.

References

[1] E. Pargoletti *et al.*, "An electrochemical outlook upon the gaseous ethanol sensing by graphene oxide-SnO_2 hybrid materials," *Appl. Surf. Sci.*, vol. 483, pp. 1081–1089, Jul. 2019.

[2] O. Kassem, M. Saadaoui, M. Rieu, and J.-P. Viricelle, "A novel approach to a fully inkjet printed SnO_2-based gas sensor on a flexible foil," *J. Mater. Chem. C*, vol. 7, no. 39, pp. 12343–12353, Sep. 2019.

[3] S. Vallejos, I. Gràcia, J. Bravo, E. Figueras, J. Hubálek, and C. Cané, "Detection of volatile organic compounds using flexible gas sensing devices based on tungsten oxide nanostructures functionalized with Au and Pt nanoparticles," *Talanta*, vol. 139, pp. 27–34, Jul. 2015.

[4] I. Polaert, L. Estel, R. Huyghe, and M. Thomas, "Adsorbents regeneration under microwave irradiation for dehydration and volatile organic compounds gas treatment," *Chem. Eng. J.*, vol. 162, no. 3, pp. 941–948, Sep. 2010.

[5] H. Yu *et al.*, "Design and analysis of ultrafast and high-sensitivity microwave transduction humidity sensor based on belt-shaped MoO_3 nanomaterial," *Sens. Actuators B, Chem.*, vol. 304, Feb. 2020, Art. no. 127138.

[6] R. Cherbanski and E. Molga, "Intensification of desorption processes by use of microwaves—An overview of possible applications and industrial perspectives," *Chem. Eng. Process.* , vol. 48, no. 1, pp. 48–58, Jan. 2009.

[7] U.S. Energy Information Administration. (Apr. 2022). *Biofuels Explained Ethanol*. [Online]. Available: https://www.eia.gov/energyexplained/biofuels/ethanol.php

[8] B. Doğan, D. Erol, H. Yaman, and E. Kodanli, "The effect of ethanol-gasoline blends on performance and exhaust emissions of a spark ignition engine through exergy analysis," *Appl. Thermal Eng.*, vol. 120, pp. 433–443, Jun. 2017.

[9] H. Man *et al.*, "How ethanol and gasoline formula changes evaporative emissions of the vehicles," *Appl. Energy*, vol. 222, pp. 584–594, Jul. 2018.

[10] V. K. Kareddula and R. K. Puli, "Influence of plastic oil with ethanol gasoline blending on multi cylinder spark ignition engine," *Alexandria Eng. J.*, vol. 57, no. 4, pp. 2585–2589, Dec. 2018.

[11] R. J. Clark and C. M. Fajardo, "Assessment of the properties of internal combustion engine lubricants using an onboard sensor," *Tribol. Trans.*, vol. 55, no. 4, pp. 458–465, Apr. 2012.

[12] Q. Xue, X. Tang, Y. Li, H. Liu, and X. Duan, "Contactless and simultaneous measurement of water and acid contaminations in oil using a flexible microstrip sensor," *ACS Sensors*, vol. 5, no. 1, pp. 171–179, Jan. 2020.

[13] A. M. Albishi, M. K. E. Badawe, V. Nayyeri, and O. M. Ramahi, "Enhancing the sensitivity of dielectric sensors with multiple coupled complementary split-ring resonators," *IEEE Trans. Microw. Theory Techn.*, vol. 68, no. 10, pp. 4340–4347, Oct. 2020.

[14] M. Saadat-Safa, V. Nayyeri, M. Khanjarian, M. Soleimani, and O. M. Ramahi, "A CSRR-based sensor for full characterization of magneto-dielectric materials," *IEEE Trans. Microw. Theory Techn.*, vol. 67, no. 2, pp. 806–814, Feb. 2019.

[15] M. A. Rafi, B. D. Wiltshire, and M. H. Zarifi, "Wideband tunable modified split ring resonator structure using liquid metal and 3-D printing," *IEEE Microw. Wireless Compon. Lett.*, vol. 30, no. 5, pp. 469–472, May 2020.

[16] B. D. Wiltshire, M. A. Rafi, and M. H. Zarifi, "Microwave resonator array with liquid metal selection for narrow band material sensing," *Sci. Rep.*, vol. 11, no. 1, p. 8598, Apr. 2021.

[17] Y. Ding, C.-S. Lee, Y. Li, Z.-Q. Wang, and G.-F. Li, "An angular displacement sensor-based active feedback open complementary split-ring resonator," *IEEE Microw. Wireless Compon. Lett.*, vol. 31, no. 9, pp. 1079–1082, Sep. 2021.

[18] A. K. Jha, A. Lamecki, M. Mrozowski, and M. Bozzi, "A highly sensitive planar microwave sensor for detecting direction and angle of rotation," *IEEE Trans. Microw. Theory Techn.*, vol. 68, no. 4, pp. 1598–1609, Apr. 2020.

[19] J. Mata-Contreras, C. Herrojo, and F. Martín, "Application of split ring resonator (SRR) loaded transmission lines to the design of angular displacement and velocity sensors for space applications," *IEEE Trans. Microw. Theory Techn.*, vol. 65, no. 11, pp. 4450–4460, Nov. 2017.

[20] J.-K. Park, T.-G. Kang, B.-H. Kim, H.-J. Lee, H. H. Choi, and J.-G. Yook, "Real-time humidity sensor based on microwave resonator coupled with PEDOT:PSS conducting polymer film," *Sci. Rep.*, vol. 8, p. 439, Jan. 2018.

[21] X. Huang *et al.*, "Graphene oxide dielectric permittivity at GHz and its applications for wireless humidity sensing," *Sci. Rep.*, vol. 8, no. 1, p. 43, Jan. 2018.

[22] S. K. Singh, P. Azad, M. J. Akhtar, and K. K. Kar, "Improved methanol detection using carbon nanotube-coated carbon fibers integrated with a split-ring resonator-based microwave sensor," *ACS Appl. Nano Mater.*, vol. 1, no. 9, pp. 4746–4755, Aug. 2018.

[23] G. Bailly, A. Harrabi, J. Rossignol, D. Stuerga, and P. Pribetich, "Microwave gas sensing with a microstrip interdigital capacitor: Detection of NH_3 with TiO_2 nanoparticles," *Sens. Actuators B, Chem.*, vol. 236, pp. 554–564, Nov. 2016.

[24] J. Rossignol, A. Harrabi, D. Stuerga, P. Pribetich, G. Bailly, and T. Leblois, "Critical influence of dielectric sensitive material and manufactured process in microwave gas-sensing: Application of ammonia detection with an interdigital sensor," *ACS Omega*, vol. 5, no. 20, pp. 11507–11514, May 2020.

[25] H. Hamzah, A. A. Abduljabar, and A. Porch, "High Q microwave microfluidic sensor using a central gap ring resonator," *IEEE Trans. Microw. Theory Techn.*, vol. 68, no. 5, pp. 1830–1838, Jan. 2020.

[26] A. Ebrahimi, J. Scott, and K. Ghorbani, "Ultrahigh-sensitivity microwave sensor for microfluidic complex permittivity measurement," *IEEE Trans. Microw. Theory Techn.*, vol. 67, no. 10, pp. 4269–4277, Oct. 2019.

[27] J. Sorocki, K. Wincza, S. Gruszczynski, and I. Piekarz, "Direct broadband dielectric spectroscopy of liquid chemicals using microwave-fluidic two-wire transmission line sensor," *IEEE Trans. Microw. Theory Techn.*, vol. 69, no. 5, pp. 2569–2578, May 2021.

[28] Z. Abbasi, P. Shariaty, M. Nosrati, Z. Hashisho, and M. Daneshmand, "Dual-band microwave circuits for selective binary gas sensing system," *IEEE Trans. Microw. Theory Techn.*, vol. 67, no. 10, pp. 4206–4219, Oct. 2019.

[29] S. Deif and M. Daneshmand, "Long array of microwave sensors for real-time coating defect detection," *IEEE Trans. Microw. Theory Techn.*, vol. 68, no. 7, pp. 2856–2866, Jul. 2020.

[30] L.-C. Fan, W.-S. Zhao, D.-W. Wang, Q. Liu, S. Chen, and G. Wang, "An ultrahigh sensitivity microwave sensor for microfluidic applications," *IEEE Microw. Wireless Compon. Lett.*, vol. 30, no. 12, pp. 1201–1204, Dec. 2020.

[31] J. W. Sanders, J. Yao, and H. Huang, "Microstrip patch antenna temperature sensor," *IEEE Sensors J.*, vol. 15, no. 9, pp. 5312–5319, Sep. 2015.
[32] A. Kumar *et al.*, "Ultrafast detection and discrimination of methanol gas using a polyindole-embedded substrate integrated waveguide microwave sensor," *ACS Sensors*, vol. 5, no. 12, pp. 3939–3948, Nov. 2020.
[33] H. Kou, Q. Tan, Y. Wang, G. Zhang, S. Su, and J. Xiong, "A wireless slot-antenna integrated temperature-pressure-humidity sensor loaded with CSRR for harsh-environment applications," *Sens. Actuators B, Chem.*, vol. 311, May 2020, Art. no. 127907.
[34] H. Zhang and K. J. Chen, "A tri-section stepped-impedance resonator for cross-coupled bandpass filters," *IEEE Microw. Wireless Compon. Lett.*, vol. 15, no. 6, pp. 401–403, Jun. 2005.
[35] G. Karimi, A. Lalbakhsh, and H. Siahkamari, "Design of sharp roll-off lowpass filter with ultra wide stopband," *IEEE Microw. Wireless Compon. Lett.*, vol. 23, no. 6, pp. 303–305, Jun. 2013.
[36] J. S. Hong and M. J. Lancaster, *Microstrip Filters for RF/Microwave Applications*. New York, NY, USA: Wiley, 2001.
[37] P. K. Singh, S. Basu, and Y. H. Wang, "Planar ultra-wideband bandpass filter using edge coupled microstrip lines and stepped impedance open stub," *IEEE Microw. Wireless Compon. Lett.*, vol. 17, no. 9, pp. 649–651, Sep. 2007.
[38] Q.-X. Chu and X.-K. Tian, "Design of UWB bandpass filter using stepped-impedance stub-loaded resonator," *IEEE Microw. Wireless Compon. Lett.*, vol. 20, no. 9, pp. 501–503, Sep. 2010.
[39] D. M. Pozar, *Microwave Engineering*, 3rd ed. Hoboken, NJ, USA: Wiley, 2005, p. 299.
[40] U. Kaatze, "Complex permittivity of water as a function of frequency and temperature," *J. Chem. Eng. Data*, vol. 34, no. 4, pp. 371–374, Oct. 1989.
[41] S. P. Singh, R. K. Jha, and D. K. Misra, "A microwave bridge method for measuring the complex permittivity of liquids," *IEEE Trans. Instrum. Meas.*, vols. IM–30, no. 4, pp. 303–305, Dec. 1981.
[42] A. P. Gregory and R. N. Clarke, "Tables of the complex permittivity of dielectric reference liquids at frequencies up to 5 GHz," Nat. Phys. Lab., Teddington, U.K., NPL Rep. CETM 33, Sep. 2001.
[43] A. H. Sihvola, "Mixing rules with complex dielectric coefficients," *Subsurface Sens. Technol. Appl.*, vol. 1, no. 4, pp. 393–415, Oct. 2000, doi: 10.1023/A:1026511515005.
[44] R. E. Ghiri, A. P. Saghati, E. Kaya, and K. Entesari, "A miniaturized contactless UWB microwave system for time-domain dielectric spectroscopy," *IEEE Trans. Microw. Theory Techn.*, vol. 65, no. 12, pp. 5334–5344, Nov. 2017.
[45] R. E. Ghiri, E. Kaya, and K. Entesari, "Time-domain dielectric spectroscopy using a miniaturized contact-based UWB system," *IEEE Trans. Microw. Theory Techn.*, vol. 66, no. 12, pp. 5863–5872, Dec. 2018.
[46] E. L. Chuma, Y. Iano, G. Fontgalland, and L. L. B. Roger, "Microwave sensor for liquid dielectric characterization based on metamaterial complementary split ring resonator," *IEEE Sensors J.*, vol. 18, no. 24, pp. 9978–9983, Dec. 2018.
[47] B. D. Wiltshire and M. H. Zarifi, "3-D printing microfluidic channels with embedded planar microwave resonators for RFID and liquid detection," *IEEE Microw. Wireless Compon. Lett.*, vol. 29, no. 1, pp. 65–67, Jan. 2019.
[48] L. Fu, J. Huang, Y. Xiang, Y. Chen, W. Gu, and Y. Wu, "A miniaturized differential microwave microfluidic sensor with high decoupling," *IEEE Microw. Wireless Compon. Lett.*, vol. 31, no. 7, pp. 909–912, Jul. 2021.
[49] Z. Abbasi, M. Baghelani, and M. Daneshmand, "High-resolution chipless tag RF sensor," *IEEE Trans. Microw. Theory Techn.*, vol. 68, no. 11, pp. 4855–4864, Nov. 2020.

Tanjir Alam (Graduate Student Member, IEEE) received the M.Tech. degree in RF and microwave engineering from IIT (ISM) Dhanbad, Dhanbad, India, in 2019. He is currently pursuing the Ph.D. degree at the Norwegian University of Science and Technology (NTNU), Trondheim, Norway.

His current research interests involve microwave sensors, MIMO antenna for 5G applications, finite-difference time-domain (FDTD), and analytical methods.

Mr. Alam has been a Student Member of the IEEE Society since 2018. He is also an Active Member of the IEEE Microwave Theory and Technology Society (MTT-S) and the IEEE Antennas and Propagation Society (AP-S).

Michael Cheffena received the M.Sc. degree in electronics and computer technology from the University of Oslo, Oslo, Norway, in 2005, and the Ph.D. degree from the Norwegian University of Science and Technology (NTNU), Trondheim, Norway, in 2008.

In 2007, he was a Visiting Researcher with the Communications Research Centre, Ottawa, ON, Canada. From 2009 to 2010, he conducted a post-doctoral study at the University Graduate Center, Kjeller, Norway, and the French Space Agency, Toulouse, France. He is currently a Full Professor with NTNU, Gjøvik, Norway. His research interests include modeling and prediction of propagation radio channels, signal processing, medium access control protocol design, antenna sensors, and sensor systems.